Appl Nanosci (2014) 4:959–966
DOI 10.1007/s13204-013-0276-z

ORIGINAL ARTICLE

Preparation and characterization of nano structured Ba_2SnO_4 as a novel photocatalyst material for the chromate reduction

S. Omeiri · N. Allalou · G. Rekhila · Y. Bessekhouad · M. Trari

Received: 7 August 2013 / Accepted: 30 September 2013 / Published online: 13 November 2013

Abstract The photo-electrochemical properties of the layered perovskite Ba_2SnO_4, prepared by nitrate route are reported for the first time. The oxide exhibits a direct optical transition at 2.98 eV, attributed to the charge transfer O^{2-}: $2p \rightarrow Sn^{4+}$: $5s$ and possesses a chemical stability over the whole pH range. The Mott Schottky plot in acidic medium is characteristic of n type conductivity with a flat band potential E_{fb} of -0.84 V_{SCE} and an electron density N_D of 1.14×10^{17} cm^{-3}. The electrochemical impedance spectroscopy reveals the bulk and grain boundaries contributions. Ba_2SnO_4 is of interest for the environmental protection. At pH 2.5, its conduction band (CB, -0.86 V_{SCE}) is below the $HCrO_4^-$ level, yielding a spontaneous reduction to Cr^{3+} under UV light. The reduction is optimized with respect to the Cr(VI) concentration. The photo reduction follows a pseudo-first-order kinetic and the data fit well the Langmuir–Hinshelwood (L–H) model with an apparent rate constant of 0.18 h^{-1} for an initial concentration of 50 ppm. The chromate reduction under solar light is studied under optimized conditions. In presence of oxalic acid, 73 % of initial concentration disappears after $\sim$2 h of irradiation.

Keywords Perovskite · Ba_2SnO_4 · Photo-electrochemical · Chromate · Solar light

S. Omeiri · N. Allalou · G. Rekhila · Y. Bessekhouad · M. Trari (✉)
Laboratory of Storage and Valorization of Renewable Energies, Faculty of Chemistry, University of Science and Technology (USTHB), B P 32, El Alia, 16111 Algiers, Algeria
e-mail: solarchemistry@gmail.com

Introduction

Environment protection has become a field of high priority because of the large scale aquatic pollution (Karunakaran et al. 2009; Gherbi et al. 2011). Unlike organic molecules, heavy metals are non-biodegradable and various methods exist for their removal, including reverse osmosis, ion exchange, electrochemical-reduction and electro-dialysis (Paul et al. 2012). However, such methods are expensive and become inefficient at low concentrations and can consequently be used as post techniques. So, the photocatalysis is a clean and cheap process and is attractive to take the relay for the water decontamination (Kaur and Pal 2012); photocatalysis has emerged as a promising solution (Hernández-Gordillo et al. 2012; Puangpetch et al. 2008). In this regard, many semiconductor (SC) oxides have been used to convert inorganic pollutants into less harmful forms, the $CuFeO_2$-CB (~ -1 V_{SCE}) is more negative than the potential of many $M^{2+/0}$ couples which can be reduced spontaneously (Nasrallah et al. 2011; Omeiri et al. 2008). The CrO_4^{2-}/Cr^{3+} potential is too anodic with respect to $CuAlO_2$-BC level to be involved in a direct electron transfer. So, CdS is used as mediator and the new heterojunction $CuAlO_2$/CdS increases the photocatalytic efficiency. Moreover, salicylic acid as hole scavenger gives the high performance among hole scavengers, and $CuAlO_2$ approaches 100 % photostability at pH 7.5 (Brahimi et al. 2012). The applications of the photocatalysis are numerous and it is the environmental aspect that we develop through the reduction of chromate, recognized as a worldwide problem (World Health Organization International Agency for Research on Cancer 1990).

Solar energy is attractive because of its abundance, inexhaustibility and consistency. With an incident power of more than 1 kW m^{-2} (AM 1) at the sea level, the solar

energy exceeds by far the energy the mankind needs. Chromate comes from industrial activities like tannery, batteries and microelectronic and is discharged in water at concentrations up to 500 ppm. It moves through the food chain and bio-accumulates in living organisms. The WHO has drastically limited the Cr(VI) concentration in water at 0.5 ppm and the effluents must be treated at the source.

On the other hand, a great interest has been paid to the elaboration of optically active materials, the key element in photocatalysis (Köferstein and Yakuphanoglu 2010;Noori et al. 2012). Oxides are privileged for photo-electrochemical (PEC) applications because of their chemical stability. In this respect, the stannates are expected to be good photocatalysts since they have CB of Sn-5*s* orbital ($\sim$4 eV below vacuum) capable to reduce any kind of inorganic ions (Omeiri et al. 2010). Comparatively, it has been reported by Fang et al. (2013) that the light-induced vapor generation at liquid-immersed metallic nanoparticles significantly enhances the photo activity. Interestingly, by increasing the incident light flux or lowering the inter-particle separation, the authors noticed the micrometer-sized bubbles resulting from the coalescence of nanoparticle-"bound" vapor envelopes.

To our knowledge, there are yet no papers on the photocatalytic activity of layered perovskites A_2SnO_4 (A = alkaline earth) and the PEC study has not been investigated before now. Ba_2SnO_4 has environmentally friendly characteristics, in addition to be low cost and chemically stable over the whole pH range (Hinatsu and Tezuka 1998). The conduction band must be positioned at energy as high as possible and barium contributes to decrease the electro affinity of the stannate. We are interesting by Ba_2SnO_4 because barium permits to increase the electro affinity leading to a large band bending, an attractive property for *n* type specimen. However, Ba_2SnO_4 is a low polaron semiconductor and the crystallite size plays a crucial role due to the increasing number of photocatalytic sites. Because of inherent defects in polycrystalline materials and low carrier mobility (Zidi et al. 2010), a large part of electron/hole (e^-/h^+) pairs are lost in the inter-grain regions, thus resulting in a poor photo activity. Therefore, we have prepared the oxide by the chemical method which has succeeded in the synthesis of homogenous powder (Wu et al. 2004) and the crystallite size becomes comparable with the diffusion length of the minority carriers. The present work deals with the chromate reduction upon UV light onto Ba_2SnO_4. The oxygen over-voltage is high on the stannates; the level O_2/H_2O is located far above the valence band and oxygen does not evolve on Ba_2SnO_4. So, the reduction is achieved in presence of oxalic acid as hole scavenger which promotes the charges separation and protects the oxide against photo corrosion (Lahmar et al. 2012; Iliev et al. 2010).

Experimental

Ba_2SnO_4 is synthesized by nitrate route. Sn (extra pure) is chemically polished with HCl (2 N), rinsed with water and dissolved in HNO_3 (9 N); $BaCO_3$ (Merck 99.9 %, dried at 250 °C) is added in stoichiometric amount and the solution is evaporated on the sand bath. The powder is ground in an agate mortar, pressed into circular discs (ϕ = 13 mm, thickness 0.5 mm) under 5 tons/cm^2 and heated at 1,100 °C; the density approximates 80 %. The completion of the reaction is checked by X-ray diffraction (XRD) using Cu Kα anticathode (λ = 0.154178 nm). The diffuse reflectance spectrum is plotted with a UV–Visible–NIR spectrophotometer (Specord plus).

The point of zero charge (pzc) is determined by measuring the equilibrium pH of an aqueous solution containing a suspension of finely powdered oxide. The sample has to be *n* type in order to be used as photoanode and this is achieved by heating the Ba_2SnO_4 pellet at 600 °C under dynamic vacuum (<1 mbar). A copper wire is fixed on the back pellet with silver cement. The pellet is isolated with epoxy resin so that the outside surface (0.70 cm^2) is exposed to the solution. Electrochemical measurements are conducted in the working solution ($HCrO_4^-$, pH 2.5) using a standard cell. A platinum foil serves as auxiliary electrode and all potentials are given with respect to a saturated calomel electrode (SCE) and controlled with a PGZ301 potentiostat (Radiometer). The frequency is set up at 10 kHz for the capacitance measurement. The electrochemical impedance spectroscopy (EIS) is measured at the open circuit potential (OCP = +0.236 V) by using small amplitude sine wave with a frequency analyzer in the range (10^{-2}–10^5 Hz).

Glassware flasks are immersed in sulfo-chromic acid overnight and rinsed with water. The stock solution (300 ppm) is prepared from $K_2Cr_2O_7$ (Merck, extra pure) in water. The concentrations down to 25 ppm are made up by dilution. The photocatalytic tests are done in a double walled Pyrex reactor containing 0.1 g of the catalyst powder in 100 cm^3 of $HCrO_4^-$ solution at variable concentrations, acidified by H_2SO_4 (pH 2.5). The chrono-potentiometric profile is recorded in the $Ba_2SnO_4/HCrO_4^-$ suspension, the potential between the Pt electrode (Tacussel) and SCE is measured with a high impedance voltammeter (Tacussel 9A). The powder is maintained in the dark (4 h) to reach the adsorption equilibrium. The temperature is regulated at 25 °C with a thermo stated bath and the experiments are performed in air-equilibrated suspension. Then, the light is switched on, UV lamp (Phywe) serves as illumination source. The precipitate is allowed to deposit in the bottom of the reactor; the solution is centrifuged (3,000 rpm, 5 min) and the residual Cr(IV) concentration is measured with the same spectrophotometer

using a 1 cm quartz cell. The efficiency of Cr(VI) photo reduction is given by:

$$\% = (A_o - A) \times 100/A_o$$

A_o and A are, respectively, the absorbance of $HCrO_4^-$ solution before and after illumination at saturation ($\sim$2 h). The solar experiments are performed on a sunny day in unstirred Pyrex reactor containing the chromate solution. The reactor is exposed to sunlight and the temperature reaches 33 °C at the end of the test. Distilled water ($\sim$0.8 MΩ cm) is used in all experiments.

Results and discussion

The synthesis of oxides by solid state reactions requires long time of heat treatment and high temperatures leading to irregular crystallite sizes with low active surface. By contrast, the chemical route yields homogenous powder with narrow size distribution (Čerňanský et al. 2002). The XRD pattern (Fig. 1) is characteristic of single phase; all peaks are indexed in the perovskite structure with a quadratic symmetry (SG: I4/mmm, JCPDS) in agreement with the JCPDS card N° 40–0010. The crystallite size ($D \sim 45$ nm) is evaluated from the full width at half maximum ($= K\lambda/\beta \cos$), where $K = 0.94$ is the shape factor and β (rd) the width of the intense XRD peak (110). Assuming spherical and non-porous crystallites, a specific surface area of $\sim 20\ m^2\ g^{-1}$ ($= 6/\rho D$) is obtained, the experimental density ($\rho = 6.40\ g\ cm^{-3}$) determined by hydrostatic method in toluene.

The optical properties are important in photo catalysis and the diffuse reflectance is used to get the gap (E_g); an accurate E_g value of 2.98 eV ($\lambda_o = 416$ nm) is obtained from the derivative curve (Fig. 2), which corresponds to the charge transfer O^{2-}: $2p \rightarrow Sn^{4+}$: $5s$. The transport

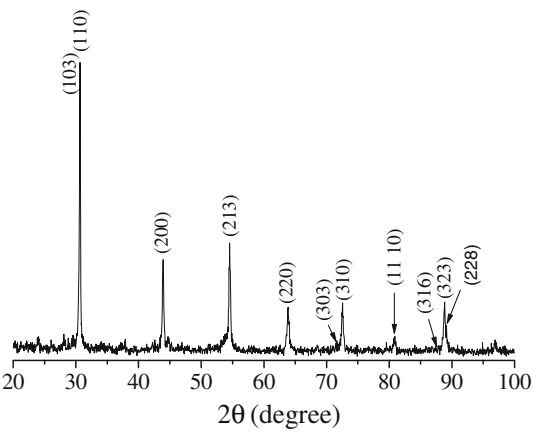

Fig. 1 XRD pattern of Ba_2SnO_4 synthesized by nitrate route at 1100 °C

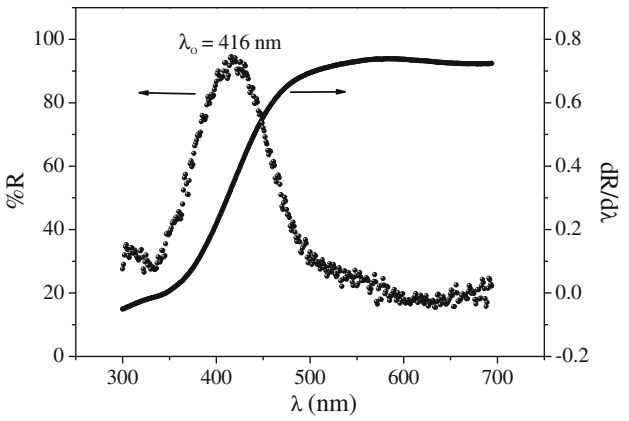

Fig. 2 The diffuse reflectance spectrum of Ba_2SnO_4 and its derivative curve

properties of the stannates are altered by oxygen deficiency (Trari et al. 1994). The system is electrically neutral and the formation of oxygen vacancies, generated by heating under vacuum, is achieved concomitantly with reduction of Sn^{4+}:

$$Ba_2SnO_4 \rightarrow Ba_2SnO_{4-\delta} + 2\delta[e^-(CB)] + \delta/2\ O_2 \qquad (1)$$

The conduction occurs by electron hopping between mixed valences $Sn^{4+/2+}$ accommodated in edge sharing octahedra. Ba_2SnO_4 is chemically stable over the whole pH range even in strong acid solutions. The intensity–potential J (V) curve in acidic medium exhibits a plateau region with a high oxygen over-voltage. The dark current is correlated to the space charge region and results from the weak electrons density (see below). The current becomes quickly large at potentials negative of $\sim$0.4 V due to hydrogen

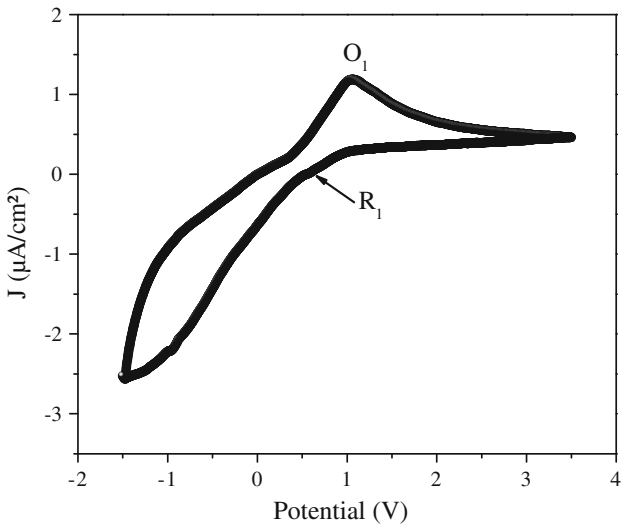

Fig. 3 Cyclic voltammogram of Ba_2SnO_4 in $HCrO_4^-$ solution (100 ppm, pH 2.5), scan rate 5 mV/s

evolution. The cathodic peak (R) and the corresponding anodic peak (O), separated by $\sim$1.3 V are due to the internal redox process $Sn^{4+/2+}$ and not to $HCrO_4^-/Cr^{3+}$ couple since the peak persists in a chromate free solution (Fig. 3). The position of the electronic bands is determined from the variation of the interfacial capacitance with the applied potential (V):

$$\frac{1}{C^2} = \left(\frac{2}{e\varepsilon\varepsilon_0 N_D}\right)(V - V_{fb}) \quad (2)$$

where ε_o is the permittivity of vacuum and e the electronic charge. The intercept of the straight line with the potential axis (Fig. 4) gives a flat band potential (V_{fb}) of -0.84 V while the positive slope lends a further support of n type conductivity. The permittivity of the material (ε–5) is determined from the dielectric measurement at 10 kHz. The linear part (C^{-2}–V) indicates a constant density (N_D) whose value (1.14×10^{17} cm^{-3}) characterizes a lightly doped semiconductor with a wide depletion width (50 nm):

$$W = \left(\frac{2\varepsilon\varepsilon_0 \Delta V}{eN_D}\right)^{0.5} \quad (3)$$

($V - V_{fb} \sim 0.35$ V) represents the optimal band bending at the interface, required for an efficient charges separation. The length W extends over many crystallographic units cells and this is advantageous in photocatalysis, since an increasing number of (e^-/h^+) pairs are separated by the junction electric field which contribute to the photoactivity. The potential V_{fb} gives the energetic position of Ba_2SnO_4-CB with respect to vacuum:

$$P = 4.75 + eV_{fb} - E_a \quad (4)$$

The P value (-0.86 V/-3.89 eV) indicates that CB is primarily made of Sn-5s orbital conferring to Ba_2SnO_4 a high reducing power under UV light. Ba_2SnO_4 is an ionic compound with a white colour and VB is made up of O^{2-}: 2p orbital, located at -6.87 eV ($P - E_g$).

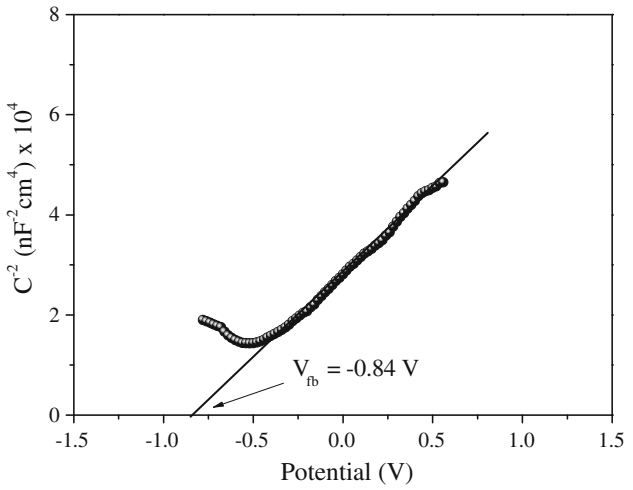

Fig. 4 The Mott–Schottky plot of Ba_2SnO_4 in the working solution ($HCrO_4^-$, 100 ppm, pH 2.5)

Photocatalysis

The solar energy continues to meet a growing demand and the photocatalysis is increasingly deployed to manage the environmental protection (Ketir et al. 2008). In view of the expensive techniques for the aquatic remediation, the exploitation of sunlight becomes highly recommended (Khataee and Kasiri 2010). Ba_2SnO_4 fills the photocatalytic requirements since it is non-toxic and chemically stable. However, it is responsive to UV light but the advantage resides in the high energy of the conduction band, able to reduce inorganic pollutant and the chromate reduction is used as test reaction. It is worthwhile to outline that the annual sunshine duration averages 12 h/day (Sahara) and more than 50 W m^{-2} of UV light is of interest for Ba_2SnO_4.

The stannates are small polaron oxides with low electron mobility (5.2×10^{-2} cm^2 V^{-1} s^{-1}).[1] Hence, the photocatalytic performance should be improved for small crystallite size (L), which must be comparable with the electron diffusion length and this can be achieved by preparing the oxide by nitrate route. The charge transfer is governed by the difference between Ba_2SnO_4-CB and $HCrO_4^-$ level. The further advantage is that Ba_2SnO_4-CB varies with pH (-0.06 V pH^{-1}) but less than $HCrO_4^-$ (0.14 V pH^{-1}) and this property has been exploited. The difference increases with decreasing pH and approaches the optimal band bending at pH 2.5, leading to an efficient separation of (e^-/h^+) pairs. With an acidity constant (pK_a) of 1.69, H_2CrO_4 predominates at low pH_s and converts to $HCrO_4^-$ above pH 1.7. The heterogeneous transfer requires a detailed knowledge of the interfacial chemistry through the junction as well as a judicious selection of the reducing agent to prevent the holes accumulation. Oxalic acid (OA) being favourable and its mineralization occurs via holes valence band process:

$$HCrO_4^- + 1.5\ C_2H_2O_4 + 4\ H_3O^+ \leftrightarrow Cr^{3+} + 3\ CO_2 + 8\ H_2O \quad (5)$$

The holes are consumed by OA, resulting in prolonged lifetime of carriers. The reactions occurring at the interface are the following:

$$Ba_2SnO_4 + h\nu \rightarrow h^+_{VB} + e^-_{CB} \quad (6)$$

$$HCrO_4^- + 7\ H_3O^+ + 3\ e^- \rightarrow Cr^{3+} + 11\ H_2O \quad (7)$$

$$3\ C_2H_2O_4 + 0.5\ O_2 + 4\ h^+ \rightarrow 6\ CO_2 + H_2O + 4\ H^+ \quad (8)$$

[1] Calculated from the $\sigma = e\ \mu_e\ N_D$.

$$2\ H_2O\ +\ 2e^-\ \rightarrow\ H_2\ +\ 2\ OH^- \quad (9)$$

The surface adsorption has a direct effect on the photoactivity, via the increasing number of the photocatalytic sites. The attachment of chromate on the catalyst powder makes easier the electron transfer. Therefore, the photocatalysis involves a dark adsorption below pzzp (= 12.7) and the enhanced activity is due simply to adsorbed $HCrO_4^-$ on the catalyst powder by electrostatic forces. Since the powder cannot be polarized, the additional criterion for the photocatalysis is that the free potential ($U_f = 0.041$ V) must be above the potential V_{fb} of n-Ba_2SnO_4 (−0.84 V). In the dark, the potential goes to cathodic values showing that the chromate adsorption takes place onto Ba_2SnO_4 and saturates at ∼230 mn (Fig. 5). Then, the light is switched on and the potential decreases again indicating the reduction of $HCrO_4^-$ into Cr^{3+}. It is worth mentioning that the photolysis $HCrO_4^-$ (without catalyst) is weak; the concentration decreases by 2 % after 4 h irradiation and no redox reaction occurs between $HCrO_4^-$ and OA Hence, the performance of Ba_2SnO_4 is a light-induced process. However, the moderate photoactivity is attributed to the small exchange current density (J_o ∼ 200 nA/cm^2) which is best though as the rate constant of electron transfer at zero potential.

The concentrations of chromate in industrial effluents can reach 300 ppm or more. Therefore, it is of interest to investigate the Cr(VI) reduction as a function of the initial concentration (C_o) in the range (25–300 ppm). The results show that the reduction decreases with increasing C_o (Fig. 6). At low concentrations the number of photocatalytic sites is more than the Cr(VI) ions and the photoactivity increases with raising C_o until saturation of all catalytic sites by $HCrO_4^-$ ion. The photons flux being constant, the chromate concentration increases and becomes greater than the number of photoelectrons, thus lowering the reduction process. The coloration of the solution also accounts for the regression in the photoactivity. Indeed, the absorption of $HCrO_4^-$ solution (50 ppm) is high over the visible region; ∼30 % of light is absorbed for 1 cm path at 350 nm. It is well established that the photocatalysis is efficient at low concentrations. Therefore, we have selected a concentration of 50 ppm for the further experiments (Mekatel et al. 2012).

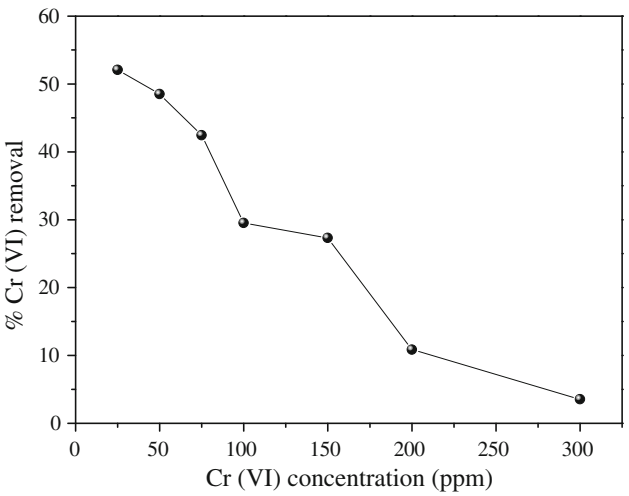

Fig. 6 The variation of the photo reduction with respect to the $HCrO_4^-$ concentration

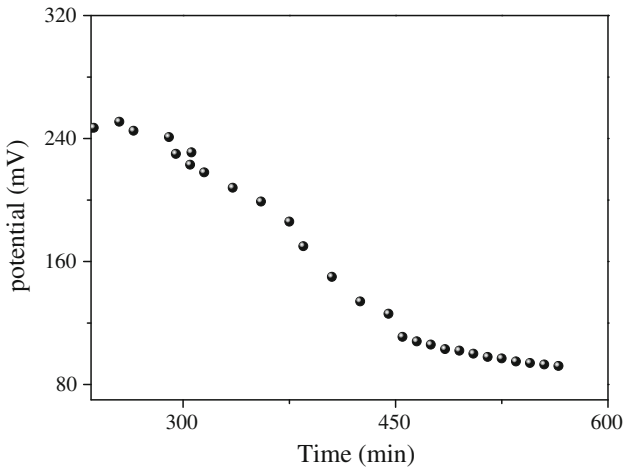

Fig. 5 The chrono-potentiometric profile of $HCrO_4^-$ solution (100 ppm) in Ba_2SnO_4 powder suspension both in the dark and under UV light

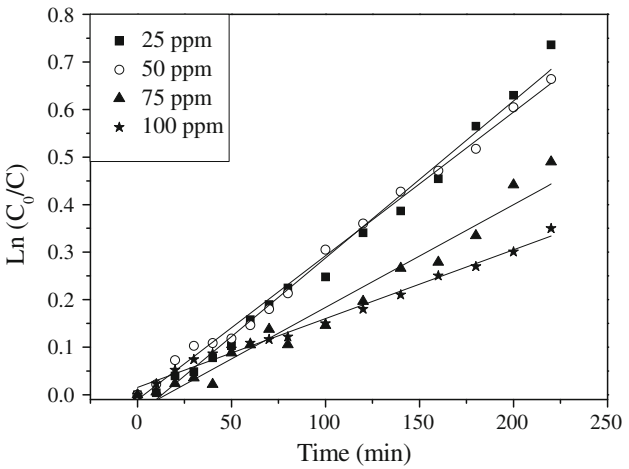

Fig. 7 Kinetics of the chromate photo reduction in presence of oxalic acid linear transform ln (C_o/C) as a function of time at different chromate concentrations (pH 2.5 $T = 25$ °C, and Ba_2SnO_4 dose = 1 mg/mL)

Table 1 The kinetic parameters of the chromate reduction according to the Langmuir–Hinshelwood

C_o (ppm)	25	50	75	100
K_{app} (min^{-1})	0.0033	0.0030	0.0021	0.0014
R^2	0.987	0.993	0.963	0.989
$t_{1/2}$	208.46	228.47	319.47	475.86

Kinetic analysis

The kinetic of the $HCrO_4^-$ reduction under illumination is given in Fig. 7. The reduction rate depends on the concentration C_o and is well described by a pseudo-first-order kinetic:

$$r = -\frac{dC}{dt} = k_{app}C \quad (10)$$

the integration gives:

$$\ln\left(\frac{C_0}{C}\right) = k_{app}t \quad (11)$$

k_{app} (mn^{-1}) is the apparent rate constant. The plot of ln (C_o/C) against the illumination time (t) for different concentrations C_o fits well the experimental data. The constants k_{app} and the correlation coefficients (R^2) are gathered in Table 1; k_{app}decrease with increasing C_o and the photo-reduction kinetic obeys to the Langmuir–Hinshelwood model (Poulios et al. 1998):

$$\frac{1}{k_{app}} = \frac{1}{k_r k_s} + \frac{C_o}{k_r} \quad (12)$$

The slope and the intercept of the linear plot of k_{app}^{-1} versus C_o (Fig. 8) give respectively the constants k_r (0.193 mg L^{-1} min^{-1}) and k_s (23.726 L mg^{-1}). The regression of the photoactivity may be due to the blocking of the catalytic sites by $Cr(OH)_3$ owing to the low solubility product ($K_s = 5.4 \times 10^{-31}$). Indeed, the color of Ba_2SnO_4 powder turns to green after the photocatalytic process, due to adsorbed hydroxide.

EIS is a powerful technique to differentiate the contributions of the grain boundaries, bulk and diffusion of the whole process. The spectrum of the junction Ba_2SnO_4/Cr(VI) solution is measured at the open circuit potential (+0.236 V). The occurrence of two semicircles in the Nyquist plot (Fig. 9) is due to the closeness of the time constants of the bulk and grain boundaries. The centers are located below the real axis due to constant phase element (CPE). CPE represents a deviation from the ideal capacitor, defined as $Z_{CPE} = [C(j\omega)^n]^{-1}$ where $-1 \leq n \leq 1$ and ω the angular frequency. The n value may be due to the non-uniform current distribution, the roughness of the electrode and defect states within the gap region. The bulk resistance ($R_b = 4.46$ kΩ cm^2) and grain boundaries resistance ($R_{gb} = 6.58$ kΩ cm^2) are due to the lack of the reversibility of the redox couple ($HCrO_4^-/Cr^{3+}$) over Ba_2SnO_4 i.e. a slow charge transfer of $HCrO_4^-$, thus corroborating the small exchange current density (J_o). The offset near the origin (1.42 kΩ cm^2) is due to the electrolyte resistance (R_{el}). The equivalent electrical circuit is established by the Zview Software (Fig. 9, inset), the absence of the Warburg diffusion implies that the overall process is kinetically governed by the electrons flow within the space charge region of Ba_2SnO_4. Indeed, the electrons move with low mobility in narrow Sn-5*s* orbital, not exceeding 2 eV (see above).

There is a great desire to extend the chromate reduction under sunlight. The experiments are conducted under direct

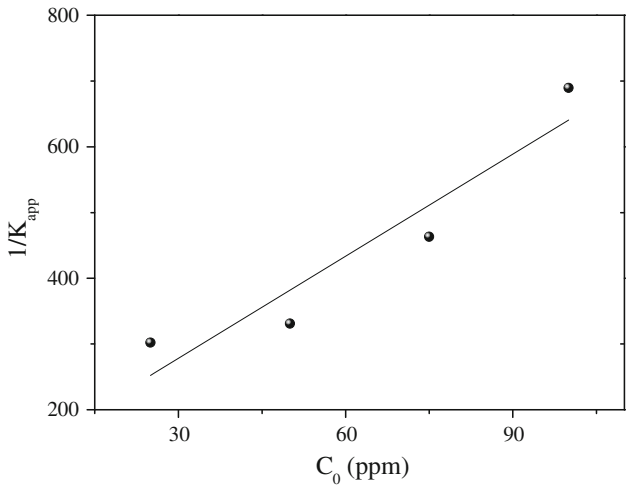

Fig. 8 The variation of $1/k_{app}$ as a function of the initial $HCrO_4^-$ concentration according to the Langmuir–Hinshelwood model. (pH 2.5, $T = 25$ °C and Ba_2SnO_4 dose = 1 mg/mL)

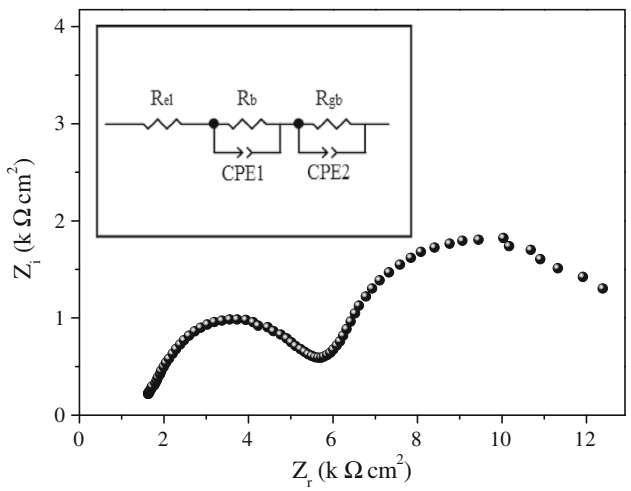

Fig. 9 The complex impedance plot of Ba_2SnO_4 in $HCrO_4^-$ solution (100 ppm) at pH 2.5. *Inset*: the equivalent electrical circuit

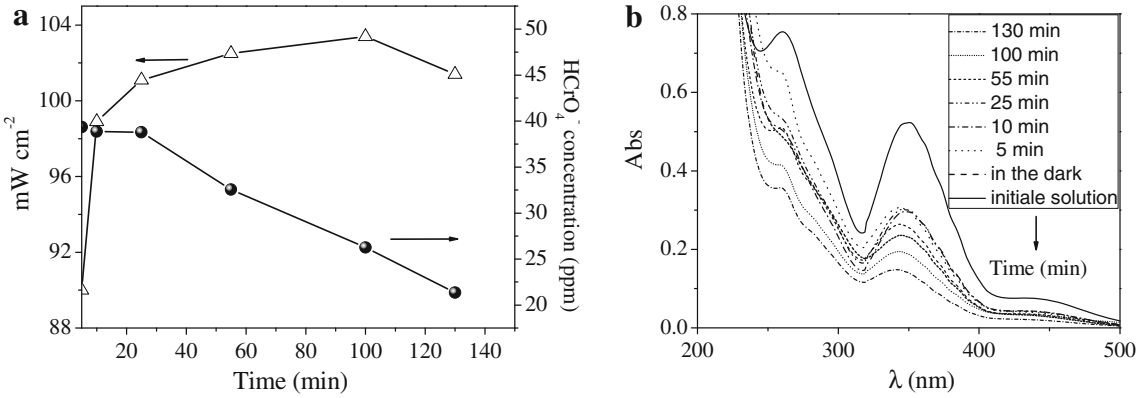

Fig. 10 **a** The effect of the light intensity on the Cr(VI) reduction. **b** The UV–Vis Spectra of the chromate solutions under sunlight on Ba_2SnO_4 over irradiation time

insulation and no correction being made from the light reflection. The light intensity varies slightly over time (Fig. 10a) and fluctuates between 90 and 103 mW cm^{-2} over the experiment duration. The temperature of the solution reached 33 °C at the end. The quantum yield (η) is defined as the number of $HCrO_4^-$ converted per incident photons[2] where $f(h\nu)$ is the photons flux density:

$$\eta = 3\{\text{number reduced of } HCrO_4^- / \text{ photons flux}\} \quad (13)$$

The number 3 is due to the fact that the reaction requires three electrons; η value of 0.13 % is obtained.

Despite its wide gap, the stannate shows an appreciable Cr(VI) photo reduction (Fig. 10b). However, the tendency to saturation over illumination time is ascribed to the competitive water reduction as observed in our previous work (Gherbi et al. 2011).

Conclusion

Cr(VI) is highly toxic and the ability of the perovskite Ba_2SnO_4 for its reduction to less harmful form is reported for the first time. Ba_2SnO_4 is safe, low cost and stable over the whole pH range. The nitrate route is employed for the preparation of homogeneous powder with fine particles. The oxide has been characterized structurally and photo-electrochemically. The conduction band is appropriately positioned with respect to the chromate level, allowing a spontaneous reduction under UV light. The low doping originating from small oxygen deficiency provides a large depletion layer with the occurrence of photo effect. The pH dependence of the flat band potential is judiciously exploited to have an optimal band bending at the interface. Concomitantly, the holes oxidize oxalic acid, thus inhibiting the charges accumulation. The best performance is achieved in acidic medium and the chromate follows a pseudo-first-order kinetic.

Acknowledgments The authors are thankful to D[r] M. Izzerouken for X-ray diffraction and M. Fedailine for thermal analysis. This research is financially supported by the Faculty of Chemistry (USTHB, Algiers).

References

Brahimi R, Bessekhouad Y, Nasrallah N, Trari M (2012) Visible light CrO_4^{2-} reduction using the new $CuAlO_2$/CdS hetero-system. J Hazard Mater 219:19–25

Čerňanský M, Přemysl V, Karel K, Radmila K (2002) A study of $PbTiO_3$ crystallization in pure and composite nanopowders prepared by the sol–gel technique. Chem Monthly 133:799–806

Fang Z, Zhen YR, Neumann O, Polman A, García de Abajo FJ, Nordlander P, Halas NJ (2013) Evolution of light-induced vapor generation at a liquid-immersed metallic nano particle. Nano Lett 13:1736–1742

Gherbi R, Nasrallah N, Amrane A, Maachi R, Trari M (2011) Photocatalytic reduction of Cr(VI) on the new hetero-system $CuAl_2O_4/TiO_2$. J Hazard Mater 186:1124–1130

Hernández-Gordillo A, Tzompantzi F, Gómez R (2012) Enhanced photoreduction of Cr(VI) using $ZnS(en)_{0.5}$ hybrid semiconductor. Catal Commun 19:51–55

Hinatsu Y, Tezuka K (1998) Electron paramagnetic resonance study of Pr^{4+}ions doped in $BaSnO_3$, Ba_2SnO_4, and $Ba_3Sn_2O_7$. J Solid State Chem 138:329–333

Iliev V, Tomova D, Rakovsky S, Eliyas A, Li Puma G (2010) Enhancement of photocatalytic oxidation of oxalic acid by gold modified WO_3/TiO_2 photocatalysts under UV and visible light irradiation. J Mol Catal A Chem 327:51–57

Karunakaran C, Panneerselvam Sujatha M, Mathisankar P (2009) Photoreduction of chromium(VI) on ZrO_2 and ZnS surfaces. Chem Monthly 140:1269–1274

[2] $\eta = \frac{\int_{Eg}^{\infty} f(h\nu)\,d(h\nu)}{\int_0^{\infty} h\nu f(h\nu)\,d(h\nu).}$

Kaur R, Pal B (2012) Size and shape dependent attachments of Au nanostructures to TiO_2 for optimum reactivity of Au–TiO_2 photocatalysis. J Mol Catal A Chem 355:39–43

Ketir W, Bouguelia A, Trari M (2008) Photocatalytic removal of M^{2+} (=Ni^{2+}, Cu^{2+}, Zn^{2+}, Cd^{2+}, Hg^{2+} and Ag^{+}) over new catalyst $CuCrO_2$. J Hazard Mater 158:257–263

Khataee AR, Kasiri MB (2010) Photocatalytic degradation of organic dyes in the presence of nanostructured titanium dioxide: influence of the chemical structure of dyes. J Mol Catal A Chem 328:8–26

Köferstein R, Yakuphanoglu F (2010) Semiconducting properties of Ge-doped $BaSnO_3$ ceramic. J Alloys Compd 506:678–682

Lahmar H, Kebir M, Nasrallah N, Trari M (2012) Photocatalytic reduction of Cr(VI) on the new hetero-system. $CuCr_2O_4$/ZnO. J Mol Catal A Chem 353:74–79

Mekatel H, Amokrane S, Bellal B, Trari M, Nibou D (2012) Photocatalytic reduction of Cr(VI) on nanosized Fe_2O_3 supported on natural Algerian clay: characteristics, kinetic and thermodynamic study. Chem Eng J 200:611–618

Nasrallah N, Kebir M, Koudri Z, Trari M (2011) Photocatalytic reduction of Cr(VI) on the novel hetero-system $CuFe_2O_4$/CdS. J Hazard Mater 185:1398–1404

Noori Sepehr M, Zarrabi M, Amrane A (2012) Removal of Cr(III) from model solutions by isolated *Aspergillus niger* and *Aspergillus oryzae* living microorganisms: equilibrium and kinetic studies. J Taiwan Inst Chem Eng 43:420–427

Omeiri S, Gabes Y, Bouguelia A, Trari M (2008) Photoelectrochemical characterization of the delafossite $CuFeO_2$: application to removal of divalent metals ions. J Electroanal Chem 6140:31–40

Omeiri S, Hadjarab B, Bouguelia A, Trari M (2010) Electrical, optical and photoelectrochemical properties of $BaSnO_{3-\delta}$: applications to hydrogen evolution. J Alloys Compd 505:592–597

Paul M, Pal N, Ali M, Bhaumik A (2012) New mesoporous silicotitaniumphosphate and its application in acid catalysis and adsorption of As(III/V), Cd(II) and Hg(II). J Mol Catal A Chem 330:49–55

Poulios I, Kositzi M, Kouras A (1998) Photocatalytic decomposition of triclopyr over aqueous semiconductor suspensions. J Photochem Photobio A Chem 115:175–183

Puangpetch T, Sreethawong T, Yoshikawa S, Chavadej S (2008) Synthesis and photocatalytic activity in methyl orange degradation of mesoporous-assembled $SrTiO_3$ nanocrystals prepared by sol–gel method with the aid of structure-directing surfactant. J Mol Catal A Chem 287:70–79

Trari M, Doumerc JP, Dordor P, Pouchard M, Behr G, Krabbes G (1994) Preparation and characterization of lanthanum doped $BaSnO_3$. J Phys Chem Solids 55:1239–1243

Wu R, Qu J, He H, Yu Y (2004) Removal of azo-dye acid red B (ARB) by adsorption and catalytic combustion using magnetic $CuFe_2O_4$ powder. Appl Catal B Environ 48:49–56

Zidi N, Omeiri S, Hadjarab B, Bouguelia A, Akroun A, Trari M (2010) Transport properties and photo electrochemical characterization of oxygen-deficient $ASnO_{3-\delta}$ (A = Ca, Sr and Ba). Phys B 405:3355–3359